NANO LETTERS

pubs.acs.org/NanoLett

Letter

# Magneto-Optical Chirality in a Coherently Coupled Exciton–Plasmon System

Samarth Vadia, Johannes Scherzer, Kenji Watanabe, Takashi Taniguchi, and Alexander Högele*

Cite This: *Nano Lett.* 2023, 23, 614–618

Read Online

ACCESS | Metrics & More | Article Recommendations | Supporting Information

**ABSTRACT:** Chirality is a fundamental asymmetry phenomenon, with chiral optical elements exhibiting asymmetric response in reflection or absorption of circularly polarized light. Recent realizations of such elements include nanoplasmonic systems with broken-mirror symmetry and polarization-contrasting optical absorption known as circular dichroism. An alternative route to circular dichroism is provided by spin-valley polarized excitons in atomically thin semiconductors. In the presence of magnetic fields, they exhibit an imbalanced coupling to circularly polarized photons and thus circular dichroism. Here, we demonstrate that polarization-contrasting optical transitions associated with excitons in monolayer $WSe_2$ can be transferred to proximal plasmonic nanodisks by coherent coupling. The coupled exciton–plasmon system exhibits magneto-induced circular dichroism in a spectrally narrow window of Fano interference, which we model in a master equation framework. Our work motivates the use of exciton–plasmon interfaces as building blocks of chiral metasurfaces for applications in information processing, nonlinear optics, and sensing.

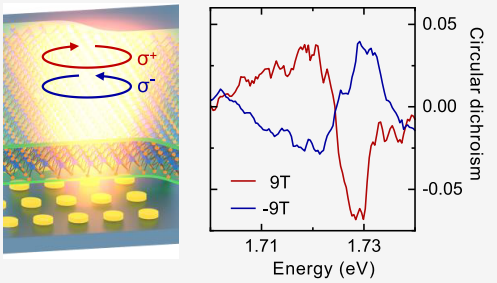


**KEYWORDS:** *two-dimensional semiconductors, metasurface, exciton–plasmon Fano coupling, magneto-induced circular dichroism*

Direct band gap and reduced dielectric screening in semiconducting monolayer transition-metal dichalcogenides (TMDs)[1,2] give rise to tightly bound excitons[3] with sizable light–matter interactions that facilitate efficient coupling to dielectric or plasmonic systems.[4−6] Capitalizing on the large oscillator strength of TMD excitons and the flexibility of combining them with plasmonic structures, recent examples of coupled exciton–plasmon systems include realizations in the strong- and weak-coupling regimes.[7−10] While the former is characterized by the formation of exciton–plasmon polaritons, the latter is distinguished by Fano-type interference spectra, as discussed in early work on various exciton–plasmon coupled systems.[11−13] In this framework, the dipolar selection rules of spin-valley polarized excitons in TMD monolayers[14−18] provide a route to chiral optical phenomena, as the valley degeneracy can be lifted by a magnetic field to induce spectrally imbalanced coupling to left- and right-handed circularly polarized photons.[19−23] This opto-valleytronic feature of TMD monolayer excitons has been utilized to demonstrate chiral effects such as directional coupling of light in silver nanowires on $WS_2$,[24] spatial separation of valley-polarized excitons by silver nanogroove arrays,[25] or second-harmonic generation of circularly polarized photons in gold-$WS_2$ metasurfaces.[26]

Here, we study magneto-optical characteristics of an exciton–plasmon metasurface based on a $WSe_2$ monolayer and gold (Au) nanodisks. We elucidate the effect of Fano interference as a function of exciton–plasmon spectral resonance detuning in the weak-coupling regime,[10,27−31] and study both experimentally and theoretically the polarization properties of the coherently coupled system in the presence of external magnetic fields. Remarkably, the coupled system exhibits magnetic circular dichroism that is distinct from the characteristics of the fundamental valley-polarized exciton transition in monolayer $WSe_2$. The resulting chiral behavior of the Fano-coupled metasurface is manifested in the form of a spectral window with polarization-dependent reflectivity in an otherwise broad-band opaque medium. The observations are substantiated by a master equation analysis with excellent quantitative agreement with experimental findings. Our work provides insight into the underlying coherent interference phenomena and can serve as a guideline for the design of exciton–plasmon metasurfaces with optical chirality in the visible spectral range.

The exciton–plasmon interface was fabricated by encapsulating a monolayer $WSe_2$ in hexagonal boron nitride (hBN) and placing the resulting heterostructure on top of a plasmonic Au nanodisk array on a $SiO_2$/Si substrate, as illustrated in Figure 1a (see Methods for sample details). The sample features regions of an encapsulated $WSe_2$ monolayer and Au

**Received:** October 31, 2022
**Revised:** December 22, 2022
**Published:** January 8, 2023

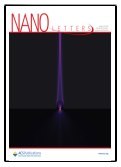





https://doi.org/10.1021/acs.nanolett.2c04246
*Nano Lett.* 2023, 23, 614–618

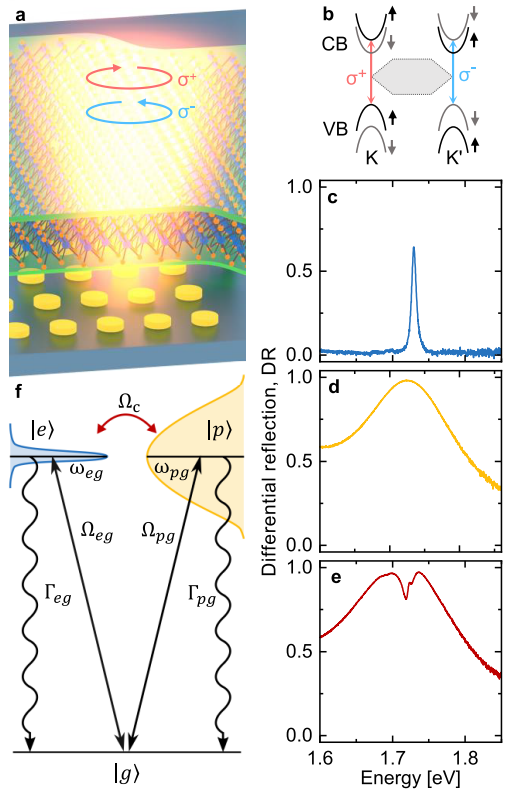


**Figure 1.** Fano interference in a coupled exciton−plasmon system. (a) Schematic illustration of monolayer $WSe_2$ encapsulated in hBN, placed on gold nanodisks and probed with circularly polarized light. (b) Band structure schematics of monolayer $WSe_2$ at two opposite corners of the hexagonal Brillouin zone, with $\sigma^+$ ($\sigma^-$) circularly polarized optical transitions between spin-up (spin-down) polarized states at the K (K′) valleys of the conduction band (CB) and valence band (VB). (c−e) Differential reflection spectra of monolayer $WSe_2$, gold nanodisk, and the coupled system, respectively. (f) Energy levels of the coupled system with $|g\rangle$, $|e\rangle$, and $|p\rangle$ denoting the ground, exciton, and plasmon states, respectively, and the corresponding exciton and plasmon optical transition frequencies $\omega_{eg}$ and $\omega_{pg}$, Rabi frequencies $\Omega_{eg}$ and $\Omega_{pg}$, and radiative decay rates $\Gamma_{eg}$ and $\Gamma_{pg}$, as well as the exciton−plasmon coupling strength $\Omega_c$.

nanodisk arrays, as well as regions where both elements are combined in vertical proximity. To characterize the optical responses of the bare exciton and plasmon systems and the regime of their coupling, we used differential reflection spectroscopy at cryogenic temperatures (see Methods for experimental details). The corresponding spectra are shown in Figure 1c−e, where the differential reflection DR = $(R_{sub} - R)/R_{sub}$ was measured relative to the reflection $R_{sub}$ of the $SiO_2$/Si substrate. The coupled system can be modeled in a three-level system framework with relevant states and rates shown in Figure 1e. The DR spectra in Figure 1c−e are representative for the excitation from the ground state $|g\rangle$ to the exciton state $|e\rangle$ with resonance and Rabi frequency $\omega_{eg}$ and $\Omega_{eg}$ and decay rate $\Gamma_{eg}$ (Figure 1c), the optical excitation to the plasmon state $|p\rangle$ with resonance and Rabi frequencies $\omega_{pg}$ and $\Omega_{pg}$ and decay rate $\Gamma_{pg}$ (Figure 1d), and the simultaneous excitation of the interacting exciton−plasmon system with coherent coupling constant $\Omega_c$ (Figure 1e).

The band structure of the $WSe_2$ monolayer is shown schematically in Figure 1b, together with polarization-contrasting optical transitions of the fundamental exciton $X^0$ in K and K′ valleys of the hexagonal Brillouin zone. The transitions are degenerate at zero magnetic field, resulting in a single Lorentzian peak in the DR spectrum of Figure 1b at $\hbar\omega_{eg} \simeq 1.723$ eV. The full-width at half-maximum (fwhm) line width of the exciton transition $\hbar\Gamma_{eg} \simeq 8$ meV is substantially smaller than the plasmon line width of $\hbar\Gamma_{pg} \simeq 180$ meV obtained from the region of a bare Au nanodisk array in Figure 1d with the resonance energy at $\hbar\omega_{pg} = 1.72$ eV. Due to variations in the dielectric environment of the nanodisk array, the plasmon resonance energy $\hbar\omega_{pg}$ varies in the range of 100 meV (see Section 1 in the Supporting Information for the description of gold nanodisk arrays). In our studies, this variation beneficially provides position-dependent spectral energy detuning $\delta = \hbar\omega_{pg} - \hbar\omega_{eg}$ of the plasmon resonance energy with respect to the exciton resonance which has negligible variations across the sample.

The spectrum of the coupled system in Figure 1e is characterized by a Fano interference line shape[27,28,32,33] with a narrow reflection dip in the broad plasmonic extinction peak. A closer inspection of the spectrum reveals an additional peak superimposed on the reflection dip, which we ascribe to the contribution from uncoupled excitons that are located within the optical spot yet sufficiently far away from plasmonic nanodisks. To interpret the resulting line shape, we inspected system realizations with different resonance detunings at different spatial positions of the interfaced array. Two representative DR spectra for negative and positive resonance detuning $\delta$ are shown in Figure 2a,b, respectively. In both spectra, the position of the dip remains essentially constant due to a small variation in the exciton energy across the sample, which also holds for the uncoupled exciton peak inside the Fano dip. Due to the asymmetric character of the Fano interference, however, the overall spectral shape is strongly modified at different resonance conditions.

We model this intricate optical response in the framework of two coherently coupled oscillators using a classical light field interacting with exciton and plasmon dipolar excitations. The dipole moments of the respective optical transitions are given as the imaginary components of the quantum coherence obtained from the master equation analysis (see Section 2 in the Supporting Information for theoretical modeling of the extinction spectrum). All main parameters of the system including the decay rates $\Gamma_{eg}$, $\Gamma_{pg}$ and the Rabi frequencies $\Omega_{eg}$, $\Omega_{pg}$ were determined from experiments on bare system components. To quantify the coupling strength $\Omega_c$, we plot the spectral position of the two maxima enclosing the dip in the Fano spectra as a function of detuning $\delta$ in Figure 2e, with their energy separation reproduced by the theoretical model for a coupling strength $\hbar\Omega_c = 28$ meV, as shown by solid lines in Figure 2e. With this coupling, our model yields the normalized extinction spectra shown in Figure 2c,d for resonance detunings $\delta = -38$ and 32 meV as extracted from the spectra in Figure 2a,b. All features of the optical response are reproduced with good agreement by the theoretical model.

With this understanding of the Fano interference phenomena, we elucidate in the following the magneto-optical response of the coupled exciton−plasmon system. First, we quantify the degree of circular dichroism (CD) associated with the exciton valley Zeeman effect in monolayer $WSe_2$.[20−23] In the presence of an out-of-plane magnetic field of 9 T, circularly polarized DR spectra of Figure 3a,b reveal two exciton resonances associated with K and K′ transitions that couple to $\sigma^+$ and $\sigma^-$ polarized light, respectively. The valley Zeeman


https://doi.org/10.1021/acs.nanolett.2c04246
Nano Lett. 2023, 23, 614−618

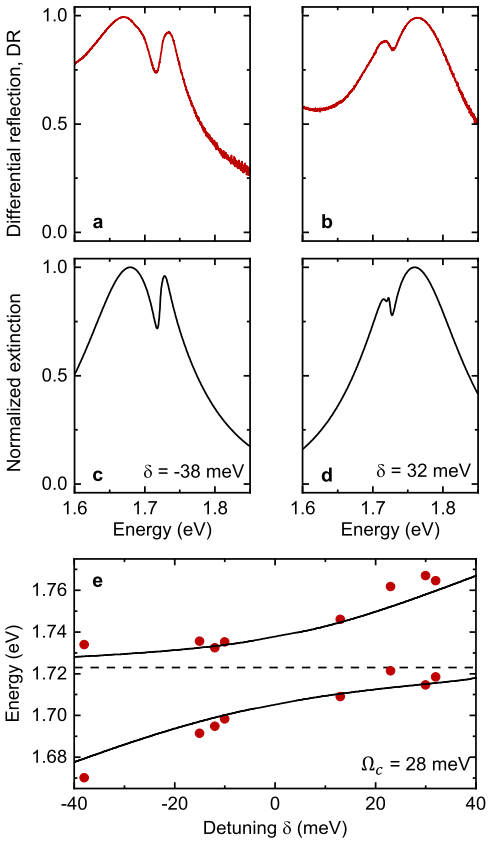


**Figure 2.** Exciton−plasmon Fano interference in experiment and theory. (a, b) Normalized differential reflection spectra of the coupled system for −38 and 32 meV energy detuning from the exciton−plasmon spectral resonance condition. The spectra were recorded on two positions of the nanodisk array with different plasmon energies $\hbar\omega_{pg}$ (determined from Lorentzian fits) for a weakly varying exciton energy $\hbar\omega_{eg}$. (c, d) Respective Fano model spectra with exciton−plasmon coupling strength $\hbar\Omega_c$ = 28 meV. (e) Evolution of the exciton−plasmon coupling as a function of resonance energy detuning $\delta$, with red data points corresponding to plasmonic array regions with different $\hbar\omega_{pg}$ and respective model results (black lines) obtained with the bare exciton energy $\hbar\omega_{eg}$ = 1.723 eV (dotted line) and $\hbar\Omega_c$ = 28 meV.

splitting of 2.1 meV corresponds to the exciton Landé factor with an absolute value of 4, as expected from previous experiments[21−23] and theory.[34−37]

The polarization-contrasting response of the two valleys is quantified by CD, which calculates as CD = $(DR^- - DR^+)/(DR^- + DR^+)$, where $DR^+$ and $DR^-$ are the $\sigma^+$ and $\sigma^-$ polarized DR spectra, respectively. Figure 3c shows the CD at 9 T as a red solid line, where $DR^+$ and $DR^-$ are the Lorentzian fits to the $\sigma^+$ and $\sigma^-$ polarized DR spectra shown as solid lines in Figure 3a,b, respectively. It shows a reversal in polarity around the resonance energy of the exciton at 0 T with a maximum CD of ∼20%. The CD obtained from the corresponding experiments at −9 T, shown in Figure 3c in blue, is reversed in sign for the entire spectral range (deviations from the mirror symmetry around the exciton energy at zero field stem from sample inhomogeneities sampled by spatial displacements in the magnetic field over a range of 18 T). All main features of the spectra are captured by our model CD spectra in Figure 3d obtained from extinction.

Next, we study the polarization-dependent optical response of the coupled system in the presence of a magnetic field. The

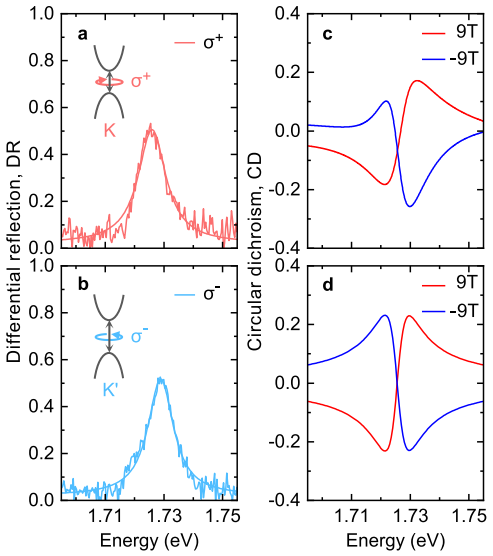


**Figure 3.** Magnetic circular dichroism of the exciton transition. (a, b) Valley-selective differential reflection spectra at 9 T for $\sigma^+$ and $\sigma^-$ polarized excitation, respectively (solid lines show Lorentzian fits). (c, d) Circular dichroism of the exciton transition at +9 (red) and −9 T (blue) from experiment and theory, respectively.

valley Zeeman effect of the bare exciton is imprinted on the exciton−plasmon system in an intricate way and is manifested as polarization-dependent reflectance. Our theory captures the experimentally observed features of the CD spectra and their evolution with the magnetic field, as evidenced by comparing experimental and theoretical data shown in Figure 4a,b and Figure 4c,d, respectively. The evolution of CD with increasing magnetic fields of 3, 6, and 9 T, recorded in the region of the Fano interference with −15 meV resonance detuning, is shown in Figure 4a. The magneto-induced dichroism becomes increasingly pronounced with increasing magnetic field as for the bare $WSe_2$ monolayer. Notably, the spectra in Figure 4c

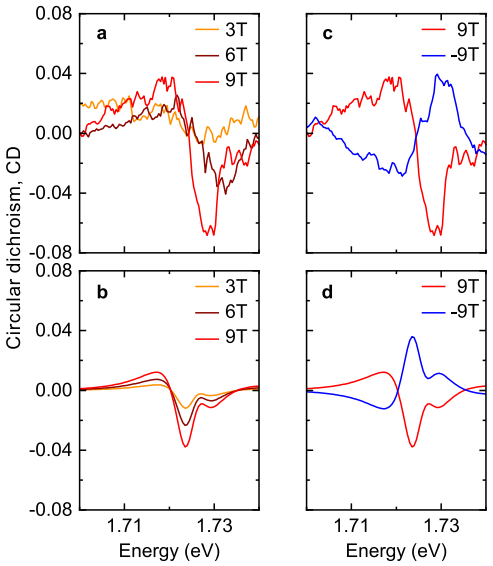


**Figure 4.** Magnetic circular dichroism of the coupled exciton−plasmon system. (a, b) Experimental and theoretical circular dichroism spectra of the coupled exciton−plasmon system at 3, 6, and 9 T. (c, d) Experimental and theoretical circular dichroism spectra in magnetic fields of +9 (red) and −9 T (blue).


https://doi.org/10.1021/acs.nanolett.2c04246
Nano Lett. 2023, 23, 614−618

show a sign reversal of the CD response for the coupled system in comparison to the bare exciton case in Figure 3c. While the monolayer features a peak in the exciton DR spectrum, the coupled exciton−plasmon spectrum is characterized by a narrow dip around the exciton resonance as a result of Fano interference, leading to reversed CD response and pronounced asymmetry for finite exciton−plasmon detunings. In the calculated spectra of Figure 4d, the asymmetry is manifested in the form of an additional dip in the CD spectra, in qualitative agreement with the experimental spectra in Figure 4c. The contribution of uncoupled excitons within the optical focal spot with a reversed sign of CD explains this observation. A maximum CD of up to ∼7% is achieved in the coupled exciton−plasmon system, indicating a significant transfer of the opto-valleytronic exciton features onto the coupled system. Consistently, the CD spectra exhibit a sign reversal at magnetic fields of ±9 T.

Our observation of magneto-optical effects in a coherently coupled exciton−plasmon system and their detailed quantitative understanding provide a pathway to design ultrathin metasurfaces for chiral spectral filtering, which could be also exploited to control nonreciprocal phenomena with the magnetic field for a unidirectional flow of circularly polarized photons as required for information transfer in quantum networks.[38,39] An obvious way to create a permanent chiral exciton−plasmon metasurface is to utilize layered ferromagnets that induce sizable exciton valley Zeeman splittings of several meV, equivalent to external magnetic fields well above 10 T.[40−44] Furthermore, the spectrally narrow response from TMD excitons in the limit of an atomically thin mirror[45−48] would yield a spectrally sharp Fano reflectance or windows of transparency in a broad extinction response. As such, spectral regions with perfect destructive quantum interference and negative refractive index equivalent to electromagnetically induced transparency could be realized for chiral slow light and information storage.[49−51]

## METHODS

The sample was fabricated by depositing monolayer $WSe_2$ (HQ Graphene) embedded in high-quality hBN (NIMS) onto a gold nanodisk array. The array was fabricated by standard electron-beam lithography and gold evaporation on a $Si/SiO_2$ substrate. All measurements were carried out at cryogenic temperatures. The data in Figures 1 and 2 were recorded in a helium bath cryostat at 4.2 K, whereas the magnetic field measurements of Figure 3 were performed in a closed-cycle magneto-cryostat (attocube systems, attoDRY1000) at 3.5 K. White-light reflection spectroscopy was performed using a halogen lamp (Ocean Optics, HL-2000) or a supercontinuum laser (NKT, SuperK Extreme EXR-4) focused to a spot of ∼1 $\mu$m diameter in a home-built confocal microscope equipped with cryogenic nanopositioners (attocube systems, ANP100 and ANP101 series) and micro-objectives (attocube systems, LT-APO/VISIR/0.82 or LT-APO/LWD/NIR/0.63). The reflected light was spectrally dispersed by a monochromator (Roper Scientific, Acton SP2500 or Acton 300i) and detected by a CCD (Roper Scientific, Spec 10:100BR/LN or Andor, iDus 416).

## ASSOCIATED CONTENT

### Supporting Information

The Supporting Information is available free of charge at https://pubs.acs.org/doi/10.1021/acs.nanolett.2c04246.

Plasmon resonance in gold nanodisk arrays, fabrication and SEM imaging of nanodisks, field intensity simulations with FDTD, coherent interference model, comparison between theory and experiment, and circular dichroism from reflection (PDF)

## AUTHOR INFORMATION


### Corresponding Author

**Alexander Högele** − *Fakultät für Physik, Munich Quantum Center, and Center for NanoScience (CeNS), Ludwig-Maximilians-Universität München, 80539 München, Germany; Munich Center for Quantum Science and Technology (MCQST), 80799 München, Germany;* orcid.org/0000-0002-0178-9117; Email: alexander.hoegele@physik.uni-muenchen.de

### Authors

**Samarth Vadia** − *Fakultät für Physik, Munich Quantum Center, and Center for NanoScience (CeNS), Ludwig-Maximilians-Universität München, 80539 München, Germany; Munich Center for Quantum Science and Technology (MCQST), 80799 München, Germany; attocube systems AG, 85540 Haar, Germany*

**Johannes Scherzer** − *Fakultät für Physik, Munich Quantum Center, and Center for NanoScience (CeNS), Ludwig-Maximilians-Universität München, 80539 München, Germany*

**Kenji Watanabe** − *Research Center for Functional Materials, National Institute for Materials Science, Tsukuba 305-0044, Japan;* orcid.org/0000-0003-3701-8119

**Takashi Taniguchi** − *International Center for Materials Nanoarchitectonics, National Institute for Materials Science, Tsukuba 305-0044, Japan;* orcid.org/0000-0002-1467-3105

Complete contact information is available at: https://pubs.acs.org/10.1021/acs.nanolett.2c04246


### Author Contributions

S.V. and J.S. contributed equally to this work.

### Notes

The authors declare no competing financial interest.

## ACKNOWLEDGMENTS

The authors thank A. O. Govorov for fruitful discussions and P. Altpeter and C. Obermayer for continuous support in the clean room. This research was funded by the European Research Council (ERC) under the Grant Agreement No. 772195 as well as the Deutsche Forschungsgemeinschaft (DFG, German Research Foundation) within the Priority Programme SPP 2244 2DMP (Project No. 443405595) and Germany's Excellence Strategy Munich Center for Quantum Science and Technology (MCQST) EXC-2111-390814868. S.V. acknowledges funding from the European Union's Horizon 2020 research and innovation programme under the Marie Skłodowska-Curie Grant Agreement Spin-NANO No. 676108. K.W. and T.T. acknowledge support from JSPS KAKENHI (Grant Nos. 19H05790, 20H00354, and 21H05233).

## REFERENCES


(1) Mak, K. F.; Lee, C.; Hone, J.; Shan, J.; Heinz, T. F. Atomically Thin $MoS_2$: A New Direct-Gap Semiconductor. *Phys. Rev. Lett.* **2010**, *105*, 136805.
(2) Splendiani, A.; et al. Emerging Photoluminescence in Monolayer $MoS_2$. *Nano Lett.* **2010**, *10*, 1271−1275.
(3) Wang, G.; et al. Colloquium: Excitons in atomically thin transition metal dichalcogenides. *Rev. Mod. Phys.* **2018**, *90*, 021001.
(4) Liu, X.; et al. Strong light-matter coupling in two-dimensional atomic crystals. *Nat. Photonics* **2015**, *9*, 30.
(5) Dufferwiel, S.; et al. Exciton-polaritons in van der Waals heterostructures embedded in tunable microcavities. *Nat. Commun.* **2015**, *6*, 8579.
(6) Schneider, C.; Glazov, M. M.; Korn, T.; Höfling, S.; Urbaszek, B. Two-dimensional semiconductors in the regime of strong light-matter coupling. *Nat. Commun.* **2018**, *9*, 2695.
(7) Liu, W.; et al. Strong Exciton−Plasmon Coupling in $MoS_2$ Coupled with Plasmonic Lattice. *Nano Lett.* **2016**, *16*, 1262−1269.
(8) Kleemann, M.-E.; et al. Strong-coupling of $WSe_2$ in ultra-compact plasmonic nanocavities at room temperature. *Nat. Commun.* **2017**, *8*, 1296.
(9) Kern, J.; et al. Nanoantenna-Enhanced Light-Matter Interaction in Atomically Thin WS2. *ACS Photon* **2015**, *2*, 1260.
(10) Lee, B.; et al. Fano resonance and spectrally modified photoluminescence enhancement in monolayer $MoS_2$ integrated with plasmonic nanoantenna array. *Nano Lett.* **2015**, *15*, 3646.
(11) Wiederrecht, G. P.; Wurtz, G. A.; Hranisavljevic, J. Coherent coupling of molecular excitons to electronic polarizations of noble metal nanoparticles. *Nano Lett.* **2004**, *4*, 2121−2125.
(12) Zhang, W.; Govorov, A. O.; Bryant, G. W. Semiconductor-metal nanoparticle molecules: Hybrid excitons and the nonlinear fano effect. *Phys. Rev. Lett.* **2006**, *97*, 146804.
(13) Govorov, A. O. Semiconductor-metal nanoparticle molecules in a magnetic field: Spin-plasmon and exciton-plasmon interactions. *Phys. Rev. B* **2010**, *82*, 155322.
(14) Xiao, D.; Liu, G. B.; Feng, W.; Xu, X.; Yao, W. Coupled spin and valley physics in monolayers of $MoS_2$ and other group-VI dichalcogenides. *Phys. Rev. Lett.* **2012**, *108*, 196802.
(15) Cao, T.; et al. Valley-selective circular dichroism of monolayer molybdenum disulphide. *Nat. Commun.* **2012**, *3*, 887.
(16) Mak, K. F.; He, K.; Shan, J.; Heinz, T. F. Control of valley polarization in monolayer $MoS_2$ by optical helicity. *Nat. Nanotechnol.* **2012**, *7*, 494−498.
(17) Zeng, H.; Dai, J.; Yao, W.; Xiao, D.; Cui, X. Valley polarization in $MoS_2$ monolayers by optical pumping. *Nat. Nanotechnol.* **2012**, *7*, 490−493.
(18) Sallen, G.; et al. Robust optical emission polarization in $MoS_2$ monolayers through selective valley excitation. *Phys. Rev. B* **2012**, *86*, 081301.
(19) Li, Y.; et al. Valley splitting and polarization by the Zeeman effect in monolayer $MoSe_2$. *Phys. Rev. Lett.* **2014**, *113*, 266804.
(20) Aivazian, G.; et al. Magnetic Control of Valley Pseudospin in Monolayer $WSe_2$. *Nat. Phys.* **2015**, *11*, 148.
(21) Srivastava, A.; et al. Valley Zeeman effect in elementary optical excitations of monolayer $WSe_2$. *Nat. Phys.* **2015**, *11*, 141.
(22) Wang, G.; et al. Magneto-optics in transition metal diselenide monolayers. *2D Mater.* **2015**, *2*, 034002.
(23) Koperski, M.; et al. Orbital, spin and valley contributions to Zeeman splitting of excitonic resonances in $MoSe_2$, $WSe_2$ and $WS_2$ monolayers. *2D Mater.* **2019**, *6*, 015001.
(24) Gong, S.-H.; Alpeggiani, F.; Sciacca, B.; Garnett, E. C.; Kuipers, L. Nanoscale chiral valley-photon interface through optical spin-orbit coupling. *Science* **2018**, *359*, 443−447.
(25) Sun, L.; et al. Separation of valley excitons in a $MoS_2$ monolayer using a subwavelength asymmetric groove array. *Nat. Photonics* **2019**, *13*, 180.
(26) Hu, G.; et al. Coherent steering of nonlinear chiral valley photons with a synthetic Au−$WS_2$ metasurface. *Nat. Photonics* **2019**, *13*, 467.
(27) Fano, U. Effects of configuration interaction on intensities and phase shifts. *Phys. Rev.* **1961**, *124*, 1866.
(28) Miroshnichenko, A. E.; Flach, S.; Kivshar, Y. S. Fano resonances in nanoscale structures. *Rev. Mod. Phys.* **2010**, *82*, 2257−2298.
(29) Abid, I.; et al. Temperature-Dependent Plasmon-Exciton Interactions in Hybrid Au/$MoSe_2$ Nanostructures. *ACS Photon* **2017**, *4*, 1653−1660.
(30) Sun, J.; et al. Light-emitting plexciton: Exploiting plasmon-exciton interaction in the intermediate coupling regime. *ACS Nano* **2018**, *12*, 10393−10402.
(31) Petric, M. M.; et al. Tuning the Optical Properties of a $MoSe_2$ Monolayer Using Nanoscale Plasmonic Antennas. *Nano Lett.* **2022**, *22*, 561.
(32) Limonov, M. F.; Rybin, M. V.; Poddubny, A. N.; Kivshar, Y. S. Fano resonances in photonics. *Nat. Photonics* **2017**, *11*, 543.
(33) Li, X.; Zhou, L.; Hao, Z.; Wang, Q.-Q. Plasmon-exciton coupling in complex systems. *Adv. Opt. Mater.* **2018**, *6*, 1800275.
(34) Woźniak, T.; Faria Junior, P. E.; Seifert, G.; Chaves, A.; Kunstmann, J. Exciton *g* factors of van der waals heterostructures from first-principles calculations. *Phys. Rev. B* **2020**, *101*, 235408.
(35) Förste, J.; et al. Exciton g-factors in monolayer and bilayer $WSe_2$ from experiment and theory. *Nat. Commun.* **2020**, *11*, 4539.
(36) Deilmann, T.; Krüger, P.; Rohlfing, M. Ab initio studies of exciton *g* factors: Monolayer transition metal dichalcogenides in magnetic fields. *Phys. Rev. Lett.* **2020**, *124*, 226402.
(37) Xuan, F.; Quek, S. Y. Valley zeeman effect and landau levels in two-dimensional transition metal dichalcogenides. *Phys. Rev. Research* **2020**, *2*, 033256.
(38) Kimble, H. J. The quantum internet. *Nature* **2008**, *453*, 1023.
(39) Reiserer, A.; Rempe, G. Cavity-based quantum networks with single atoms and optical photons. *Rev. Mod. Phys.* **2015**, *87*, 1379.
(40) Zhong, D.; et al. Van der waals engineering of ferromagnetic semiconductor heterostructures for spin and valleytronics. *Sci. Adv.* **2017**, *3*, No. e1603113.
(41) Zhao, C.; et al. Enhanced valley splitting in monolayer wse2 due to magnetic exchange field. *Nat. Nanotechnol.* **2017**, *12*, 757−762.
(42) Seyler, K. L.; et al. Valley manipulation by optically tuning the magnetic proximity effect in $WSe_2/CrI_3$ heterostructures. *Nano Lett.* **2018**, *18*, 3823.
(43) Norden, T.; et al. Giant valley splitting in monolayer $WS_2$ by magnetic proximity effect. *Nat. Commun.* **2019**, *10*, 4163.
(44) Ciorciaro, L.; Kroner, M.; Watanabe, K.; Taniguchi, T.; Imamoglu, A. Observation of Magnetic Proximity Effect Using Resonant Optical Spectroscopy of an Electrically Tunable $MoSe_2$/$CrBr_3$ Heterostructure. *Phys. Rev. Lett.* **2020**, *124*, 197401.
(45) Bettles, R. J.; Gardiner, S. A.; Adams, C. S. Enhanced optical cross section via collective coupling of atomic dipoles in a 2d array. *Phys. Rev. Lett.* **2016**, *116*, 103602.
(46) Zeytinoglu, S.; Roth, C.; Huber, S.; Imamoglu, A. Atomically thin semiconductors as nonlinear mirrors. *Phys. Rev. A* **2017**, *96*, 031801.
(47) Shahmoon, E.; Wild, D. S.; Lukin, M. D.; Yelin, S. F. Cooperative resonances in light scattering from two-dimensional atomic arrays. *Phys. Rev. Lett.* **2017**, *118*, 113601.
(48) Back, P.; Zeytinoglu, S.; Ijaz, A.; Kroner, M.; Imamoglu, A. Realization of an electrically tunable narrow-bandwidth atomically thin mirror using monolayer mose$_2$. *Phys. Rev. Lett.* **2018**, *120*, 037401.
(49) Boller, K.-J.; Imamoglu, A.; Harris, S. E. Observation of electromagnetically induced transparency. *Phys. Rev. Lett.* **1991**, *66*, 2593.
(50) Hau, L. V.; Harris, S. E.; Dutton, Z.; Behroozi, C. H. Light speed reduction to 17 meters per second in ultracold atomic gases. *Nature* **1999**, *397*, 594.
(51) Lukin, M. D.; Imamoglu, A. Controlling photons using electromagnetically induced transparency. *Nature* **2001**, *413*, 273.



https://doi.org/10.1021/acs.nanolett.2c04246
*Nano Lett.* 2023, 23, 614−618